Available online at www.sciencedirect.com
SCIENCE DIRECT
Journal of Molecular Catalysis A: Chemical 246 (2006) 146–153
JOURNAL OF MOLECULAR CATALYSIS A: CHEMICAL
www.elsevier.com/locate/molcata

Theoretical modeling of molecular interactions of iron with asphaltenes from heavy crude oil

Sergio Rosales [a], Iván Machín [b], Morella Sánchez [a,c], Guaicaipuro Rivas [b], Fernando Ruette [a,*]

[a] *Lab. de Química Computacional, Instituto Venezolano de Investigaciones Cientificas (IVIC), Apdo. 21827, Caracas 1020-A, Venezuela*
[b] *INTEVEP, Edo. Miranda, P.O. Box 76343, Caracas 1070-A, Venezuela*
[c] *Departamento de Química, Instituto Universitario de Tecnología Federico Rivero-Palacio, Apartado 40347, Caracas, Venezuela*

Received 19 August 2005; received in revised form 25 October 2005; accepted 25 October 2005
Available online 1 December 2005

Abstract

The interaction of metallic iron with a model asphaltene molecule in the presence of water and electron-donor additives was modeled by using a quantum mechanics parametric method, CATIVIC. Results of Fe–asphaltene interactions show the formation of bonds on aromatic rings and directly on heteroatoms and so a decrease of C─C, N─C, and S─C bond energies (bond activations) and the formation of metal–asphaltene complexes. Values of diatomic energies (DE), equilibrium bond distances (EBD), and diatomic bond energies (DBE) show that the most significant bonds arise when the interaction is directly on heteroatoms (N, S) and the highest activation is in the C─S bonds. Electronic charge transfer occurs from the metal to hydrocarbon, except when interaction is on the N atom. Important metal─O bond is observed when water interacts with Fe–asphaltene complex, leading to some activation of O─H bonds. Negative charge on the system, in the presence of H_2O, will decrease Fe─O and Fe─N bonds and will reinforce Fe─S ones. Comparison with previous work shows that, in general, hydrogenation and carbon–heteroatom bond activations due to metal interaction in the presence of water follow the trend: nickel > iron.

Keywords: CSC; Iron catalyst; Asphaltene; CATIVIC; Heavy crude oil; Catalytic modeling

1. Introduction

Important components of heavy oil (HO) are asphaltene molecules that contain polyaromatic rings with side chains. They exist as monomer and micelles that are in colloidal range. Asphaltene flocculation could have detrimental effects on oil production, transportation, and refinery process. The necessity of discovering new treatments for HO comes from the need to transform low quality oil with high contents of impurities, such as heteroatoms (metals, sulfur, and nitrogen), into a more valuable material. Clean fractions of oil also avoid environmental pollution by elimination of refractory sulfur and nitrogen compounds and prevent refinery catalysts poisoning by metal deposition. In addition, conventional extra-heavy crude fractions and refinery petroleum residues have a high viscosity with the tendency to form coke and to precipitate. This also results in a catalyst poisoning and deactivation. All of these undesirable characteristics require special physical and chemical treatments for HO before or during refining process.

Transition metals are widely used as standard oil refining catalysts for breaking C–C, C–H, and H–H bonds. Recently, important technical advances have been carried out combining conventional thermal treatment and catalytic processes that promote low cost hydrogen addition to unsaturated hydrocarbons [1,2]. An improvement of heavy and extra-heavy crude oil using steam has limitations in the low hydrogenation capacity and therefore the bond saturation with hydrogen after cracking to produce light fractions of oil. Actually, several processes including the steam cracking, steam reforming, carbon gasification, and catalytic steam cracking [3,4] have been used to produce light oil. The main idea is to update extra-heavy crude oil by using abundant and cheap hydrogen-rich molecules (water, methane, ammonia, etc.) to partially transfer hydrogen

* Corresponding author. Tel.: +58 212 5041442; fax: +58 212 5041350.
E-mail address: fruette@ivic.ve (F. Ruette).

1381-1169/$ – see front matter © 2005 Elsevier B.V. All rights reserved.
doi:10.1016/j.molcata.2005.10.027

to heavy molecules (asphaltenes), generating light oil fractions and avoiding condensation and polymerization reactions that lead to coke production. In this sense, hydrocarbon hydrogenation at low-pressure water plasma has been reported by Patiño and co-workers [5].

In previous work [6], the interaction of Ni with a model HO asphaltene molecule without and with water was evaluated with CATIVIC method. A reaction scheme was proposed for a catalytic steam cracking (CSC) process based on the formation and breaking of bonds. Results showed important metal–hydrocarbon interactions especially between sites that contain N and S atoms in the asphaltene molecule. The formation of nickel–asphaltene intermediate complexes was proposed. Some nickel–asphaltene complexes were able to dissociate water and hydrogenate the asphaltene molecules. It was also found that a negative charge on asphaltene–metal systems (simulation of electron transfer from potassium to asphaltene) promotes the H_2O dissociation on adsorbed Ni and favors C–S and C–N bond activations.

As far as we know, the Fe–asphaltene interaction study has not been performed yet. In this work, parametric quantum mechanical calculations were carried out in order to analyze the CSC process using a model molecule of HO (asphaltene) in the presence of a Fe atom and a water molecule. New insights of the Fe CSC activity are proposed based on qualitative results from these calculations.

This publication is organized in the following way: (a) in the next section, a brief description of the theoretical method parameterization and the feasibility of using a very simple model for the CSC reaction are presented. (b) Discussion of results is shown in Section 3 by means of an analysis of calculated asphaltene fragments (F1 and F2) properties, Fe adsorbed on different sites of these asphaltene fragments ([F1–Fe]^q and [F2–Fe]^q; q are charges, 0 and −1), and water interacting on Fe–asphaltene complex ([F1–FeH_2O]^q and [F2–FeH_2O]^q). A comparison between results of Ni and Fe metal is also presented in this section. (c) Finally, a resume of the most remarkable results and some recommendations for future works are exposed in Section 4.

2. Computational details

Calculations were carried out with a quantum chemistry parametric method named CATIVIC [7,8] employed to model catalytic and molecular systems [9–11]. This method is based on simulation techniques to mimic the total energy functional using basic parametric functionals [12–14]. Details of atomic and molecular parameterization processes used in this method are presented elsewhere [7,8].

Atomic parameters for H, O, C, N, and S and molecular parameters for H–H, H–O, H–C, H–N, H–S, C–O, C–N, C–S, C–C, N–O, N–S, N–N, and S–S are taken from MINDO/SR method [15]. Values for Fe atomic parameters were gotten from Reference [16]. Molecular parameters alpha and beta for Fe–O and Fe–H were acquired from previous works [16,17]. Parameters for Fe–S, Fe–N, and Fe–C bonds were adjusted to obtain dissociation energy of diatomic molecules [18–20] and geometry of polyatomic molecules FeS_2, FeS_2^+, $SFeS^-$, SFe–S [21], FeNO [22], Fe–N–N^+, NFeN, N–N–Fe–N–N, FeCO [23], and $Fe(CO)_5$ [24]. The γ_{XY} term (X = Fe; Y = S, N, C) is the core–core repulsion functional [25]. It was adjusted in order to obtain the best geometry for diatomic and polyatomic molecules mentioned above. The average value of error with respect to experimental results was about 0.1 Å; therefore, results discussed here are qualitative. The optimal values of parameters (beta (β) for the electronic and alpha (α) for the core–core interaction functionals) are reported in Table 1.

Table 1
Molecular parameters beta (β) and alpha (α) for Fe—Y (Y = S, N, C)

Parameters pair of Fe—Y atoms	β_{Fe-Y}	α_{Fe-Y}
Fe—S	0.356579	0.986414
Fe—N	0.749026	1.505872
Fe—C	0.519365	0.920117

Theoretical tools used for evaluating the bond strengths: diatomic energies (DE) and diatomic bond energies (DBE) are reported elsewhere [26,27] and they come from a natural total energy partition of parametric methods.

As in previous work [6], simple models were selected to simulate the CSC reaction components, i.e., an average asphaltene molecule that characterizes the Tia Juana Venezuelan heavy crude oil; an iron atom to mimic the transition metal catalyst site; a water molecule to imitate the steam; a negative charge to simulate the electronic transfer from an alkali metal to the asphaltene molecule.

The model molecule of asphaltene was acquired from Reference [28] (see Fig. 1) and it was divided in several fragments, as in previous work [6]. The selection of F1 and F2 fragments (see Fig. 1) was carried out based on the heteroatom location (N, S). This is very important for hydrodesulfurization (HDS) and hydrodenitrogenation (HDN) process of HO.

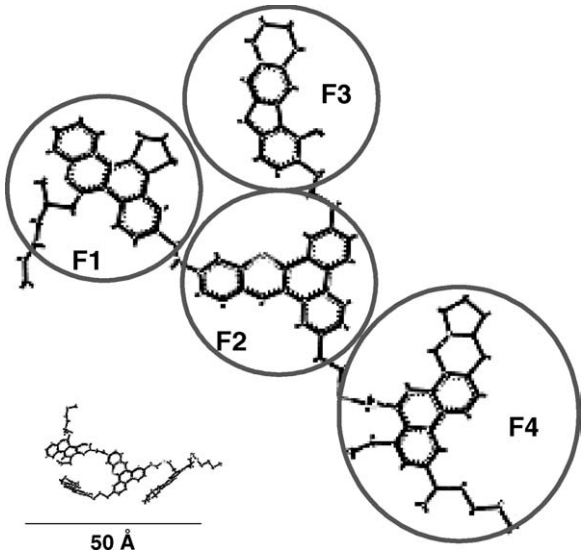

Fig. 1. Average asphaltene molecule from Tia Juana Venezuelan heavy crude oil.

3. Results and discussion

3.1. Interaction of Fe with fragment F1

Evaluation of adsorbate–substrate interactions (metal–asphaltene) was carried out for different situations. The active site catalyst (Fe) interacts on different asphaltene sites (A–F) of F1 and F2 fragments, as shown in Fig. 2. In addition, interactions were performed with and without the presence of electron-donor promoters, simulated by using neutral and negatively charged systems, respectively. A search for different spins multiplicities was carried for the neutral and charged systems. Values for the most stable multiplicities were 5 for both $[F1–Fe]^0$ and $[F2–Fe]^0$, and 6 for $[F1–Fe]^{-1}$ and $[F2–Fe]^{-1}$ systems.

The structure of the complex $[F1–Fe]^0$ with the iron adsorbed on site A is shown in Fig. 3a. DBE values for selected bonds of neutral and charged systems are presented in Table 2. In order to evaluate the effects of adsorbate–substrate interaction process, DBEs for C–C and C–N were analyzed in F1 and $[F1–Fe]^0$ systems. Comparison of C–X (X = C, N) bonds in $[F1–Fe]^0$ and F1 reveals that all of the bonds, around the adsorption site, are weakening, due to Fe–C and Fe–N interactions. In particular, the C–N and C(34)–C(32) bonds are fairly activated because they go from about −113 and −116 to −94 and −90 kcal/mol, respectively. This is also reflected in a decrease of DE and an enlargement of C–N and C–C bonds (see values of EBD). It may be concluded that Fe–asphaltene interaction may help to facilitate the C–C and C–N bond breaking by activation of these bonds (hydrocarbon cracking). These findings are supported by inductively coupled plasma/selected-ion flow tube (ICP/SIFT) tandem mass spectroscopy experiments carried out by Caraiman and Bohme [29]. They found that benzene C–C and C–H bonds are activated in gas-phase reactions with transition metal cations.

Results also indicate that the formation of a $[F1–Fe]^0$ complex in site A is possible due to Fe–C(*i*) and Fe–N inter-

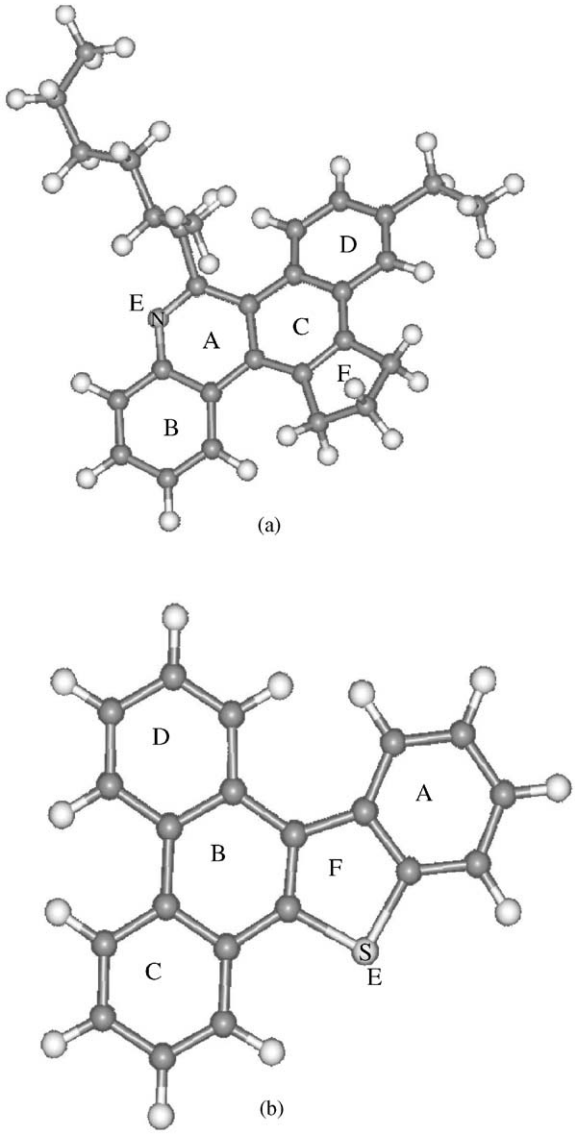

Fig. 2. Adsorption sites for Fe interaction on different fragments of asphaltene molecule: (a) fragment F1 and (b) fragment F2. White and dark balls without labels are H and C atoms, respectively.

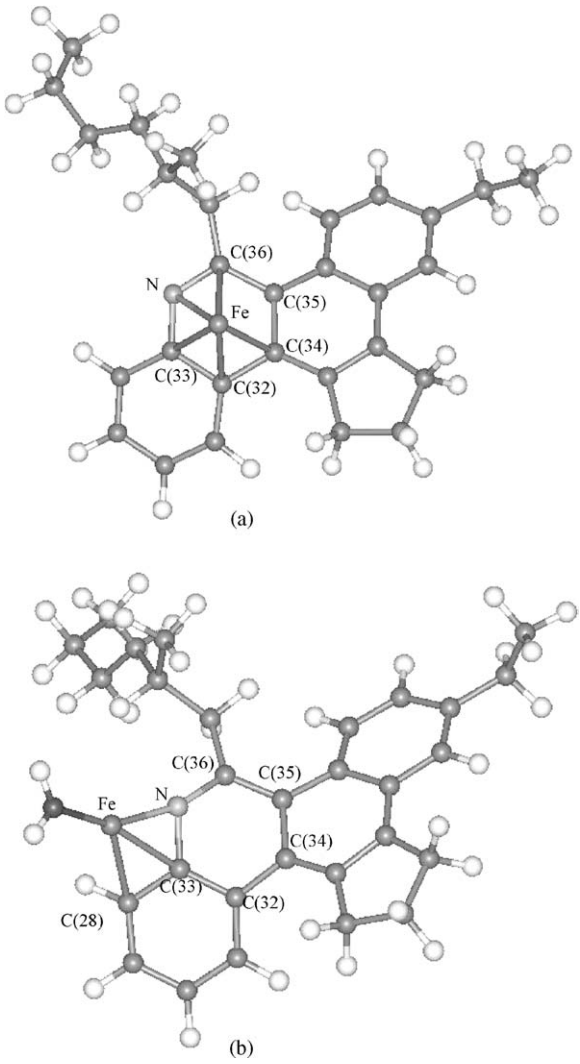

Fig. 3. (a) Adsorption mode of Fe on site A of fragment F1. (b) Final location of water molecule and Fe after interaction with H_2O–$[F1–Fe]^0$. Note that Fe was initially on site A.

Table 2
Selected DEs (a.u.), EBDs (Å, in parentheses), and DBEs (kcal/mol, in brackets) for interactions of Fe on site A of the F1 fragment with and without a water molecule (see Fig. 3)

Bonds	F1	$[F1–Fe]^0$	$[F1–Fe]^{-1}$	$[F1–FeH_2O]^0$	$[F1–FeH_2O]^{-1}$
Fe─C(32)	–	−0.107 (2.266) [−26.7]	−0.090 (2.322) –	0.003 (3.502) [0.8]	−0.088 (2.279) –
Fe─C(33)	–	−0.106 (2.306) [−25.9]	−0.122 (2.292) –	−0.103 (2.216) [−23.4]	−0.092 (2.280) –
Fe─C(34)	–	−0.126 (2.217) [−30.6]	−0.126 (2.228) –	−0.001 (4.208) [−0.2]	−0.305 (2.001) –
Fe─C(35)	–	−0.062 (2.466) [−15.6]	−0.067 (2.418) –	−0.001 (4.243) [−0.2]	0.007 (2.829) –
Fe─C(36)	–	−0.103 (2.338) [−25.4]	−0.118 (2.282) –	0.008 (3.258) [1.9]	−0.006 (2.749) –
Fe─C(28)	–	0.003 (3.517) [0.7]	0.010 (3.520) –	−0.103 (2.311) [−24.5]	0.004 (3.492) –
Fe─N	–	−0.145 (2.243) [−34.9]	−0.155 (2.202) –	−0.506 (1.908) [−110.0]	−0.341 (2.038) –
N─C(33)	−0.682 (1.305) [−112.9]	−0.587 (1.400) [−89.9]	−0.608 (1.398) –	−0.504 (1.461) [−71.2]	−0.524 (1.454) –
C(34)─C(32)	−0.657 (1.429) [−115.9]	−0.579 (1.513) [−93.5]	−0.556 (1.528) –	−0.601 (1.492) [−110.5]	−0.490 (1.573) –
Fe─O	–	–	–	−0.321 (2.093) [−72.7]	−0.312 (2.097) –
O─H(1)	–	–	–	−0.488 {−0.519} (0.952) {0.948} [−67.9] {−110.9}	−0.488 (0.952) –
Iron charge	–	0.10	0.04	0.03	0.04

Values for O─H bond in the free H_2O are given aside in braces.

actions (i = 32–36). Fe–C(i) bond strength (DBEs) are of the order of −16 to −31 kcal/mol, while the strongest interaction of −35 kcal/mol is for Fe–N bond. These qualitative results are supported by experimental facts that evidence a significant interaction between iron particles adsorbed on activated-carbon support [30]. Furthermore, Armentrout and co-workers [31] found considerable thermochemical interaction in metal–$(C_6H_6)_x^+$ complexes (x = 1 and 2) by using Xe collision-induced dissociation (CID) in a guide ion beam mass spectrometer. In addition, theoretical calculations with DFT approach indicate that Fe–arene interactions are strong as well as in the neutral and the positively charged metal atoms [32,33]. Similar results were found earlier by Bauschlicher et al. [34] for metal cations, using modified coupled-pair functional (MCPF) approach and double zeta plus polarization (DZP) basis set.

Note that the DBE values for negatively charged systems were not included here, because it requires the monoatomic energy for charged atoms [27]. The Fe^- system is not well represented for our parameterization approach. It will require the inclusion of Fe electron affinity in the evaluation of atomic Fe parameters. However, the comparison of bond strengths can be analyzed through the calculation of DE values, shown in Table 2. One can observe that the electronic charge donation (negatively charged systems), in general, slightly increases bond strengths between the asphaltene ring and Fe. This trend is in agreement with experimental observations of Schwarz and co-workers [35] using mass spectrometry in cationic arene–transition metal complexes. They reported that electron-donating groups increase the metal–arene bond dissociation energies.

Equilibrium bond length values are displayed in parentheses in Table 2. A correlation between bond lengths and DE values is observed, i.e., a long bond length implies a weak bond strength and vice versa. With respect to the atomic charges, shown in the last row of Table 2, an electronic charge transfer from the metal to the aromatic ring (0.10 a.u.) is observed, inclusive also in the case of $[F1–Fe]^{-1}$ system (0.04 a.u.). The charge transfer from metal particles to carbon has been reported by Hegenberger et al. [30] by using Mössbauer spectroscopy.

Interaction on other sites of fragment F1, in which Fe is directly anchored above the aromatic ring (sites B–D), have been considered (see Fig. 2a). The differences in energies between sites A, B, C, and D are small, site C being slightly more stable. There is in all cases an electronic charge withdrawing from Fe atom to the hydrocarbon and activation of some C–C bonds. A very good agreement with respect to other calculations is obtained, i.e., the distance from the metal to the ring center (about 1.73 Å) compares well with DFT level calculations of Fe–benzene complex performed by Pandey et al. [32] (1.72 Å). For reasons of space, a detail analysis of these adsorptions is not performed here. However, in the next subsection, an equivalent adsorption on an aromatic ring with six carbons (site A of fragment F2) is analyzed in some detail.

A site above the center of a five-atom ring was contemplated (site F). Results indicate, however, that Fe–F1 interaction in this site is repulsive, because of an important repulsion of Fe with the H atoms that point out of the ring plane. Note that this ring is partially saturated.

Calculations that correspond to a Fe lateral interaction with the N atom of fragment F1 (site E) were considered. The final location of Fe after geometrical optimization is shown in Fig. 4. Here, a different bond pattern with respect to site A is observed. A list of DBE values is presented in Table 3 in brackets. Results show strong Fe–N bonding interaction of about −72 kcal/mol and smaller ones of −28 and −19 kcal/mol for Fe–C(28) and Fe–C(33), respectively. The strong Fe–N interaction points toward a shorter equilibrium bond distance (EBD; 2.057 Å) than that in site A (2.243 Å) (see Tables 3 and 2, respectively). These bonding interactions also lead to a weakening or activation of the N–C(33) bond in Fe–F1 with respect to F1. Values of DBEs go from −113 to −82 kcal/mol and EBDs from 1.305 to 1.418 Å (see Table 3).

Electronic charge transfer occurs in an inverse way, i.e., from the hydrocarbon to the metal. The N lone pairs in the hydrocarbon donate electronic charge to the metal, as basic characteristics of the pyridinic functional group (see values in the last row of Table 3).

Table 3
DEs (a.u.), EBDs (Å), and DBE (kcal/mol) for interactions of Fe on site E of the F1 fragment with and without a water molecule (see Fig. 4)

Bonds	F1	$[F1–Fe]^0$	$[F1–Fe]^{-1}$	$[F1–FeH_2O]^0$	$[F1–FeH_2O]^{-1}$
Fe─N	–	−0.331 (2.057) [−71.7]	−0.386 (1.997) –	−0.506 (1.909) [−95.3]	−0.364 (2.032) –
Fe─C(28)	–	−0.122 (2.257) [−28.3]	−0.088 (2.357) –	−0.103 (2.270) [−23.4]	−0.048 (2.585) –
Fe─C(33)	–	−0.079 (2.335) [−18.6]	−0.096 (2.328) –	−0.113 (2.259) [−17.9]	−0.065 (2.510) –
N─C(33)	−0.682 (1.305) [−112.9]	−0.556 (1.418) [−81.5]	−0.551 (1.427) –	−0.504 (1.457) [−73.3]	−0.564 (1.417) –
C(33)─C(28)	−0.705 (1.395) [−121.0]	−0.632 (1.469) [−103.1]	−0.658 (1.457) –	−0.668 (1.456) [−106.8]	−0.672 (1.450) –
Fe─O	–	–	–	−0.321 (2.097) [−63.1]	−0.262 (2.145) –
O─H(1)	–	–	–	−0.488 (0.952) [−68.5]	−0.490 (0.952) –
Iron charge	–	−0.16	−0.28	0.44	−0.43

Values of EBDs for selected bonds are in parentheses and DBEs are in brackets.

For negatively charged systems, values of DEs in Table 3 indicate that the Fe–asphaltene bonding interaction is reinforced, particularly the Fe–N bond. The Fe–N distance changes from 2.057 to 1.997 Å and DE from −0.331 to −0.386 a.u. for neutral and charged systems, respectively. The N–C bond is slightly more activated than in the neutral case.

3.2. Interaction of Fe with fragment F2

A similar study carried out for F1 fragment was also performed for the F2 fragment. Several Fe–F2 complexes were evaluated for Fe interaction on different sites (A–F) shown in Fig. 2b. Values of DBEs for site A (see Fig. 5a) are presented in Table 4. Results indicate that interaction is mainly with the four C atoms (C(1), C(2), C(5), and C(6)) that are not forming part of the adjacent thiophenic ring. Bond interactions for Fe–C are ranging around −24 to −17 kcal/mol. Small C–C bond activations are also observed from about −131 to −109 kcal/mol. Note that although C(4) and C(3) have a very small interaction with Fe, they are in some way affected (−115 to −103 kcal/mol) because of indirect effects caused by the loss of ring aromaticity. Electronic charge transfer from the metal to the aromatic ring also occurs as in adsorption of Fe on F1 fragment, from Fe to the F2 fragment.

The presence of an electron-donor promoter (negatively charged system) leads to slightly stronger Fe–C interactions (see DE values) and shorter EBD(Fe–C) values than in the neutral system, as shown in Table 4. This also causes a small weakening and enlargement of many C–C bonds.

Results on six-center sites (B–D) are slightly different to that of $[F1–Fe]^0$ case in site A, for that reason results are not shown here in details. The interaction on C and D sites is with all C atoms of the benzene-like ring, but on B site shows a very weak interaction with carbon atoms that belong to the thiophenic ring, as in site A.

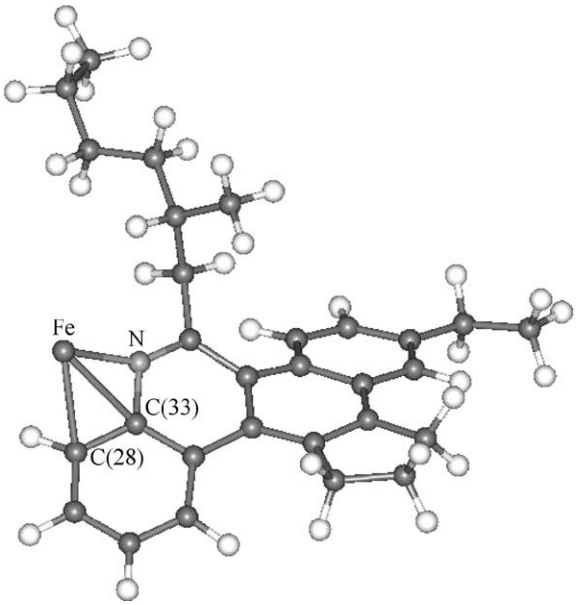

Fig. 4. Adsorption mode of Fe on site E of fragment F1.

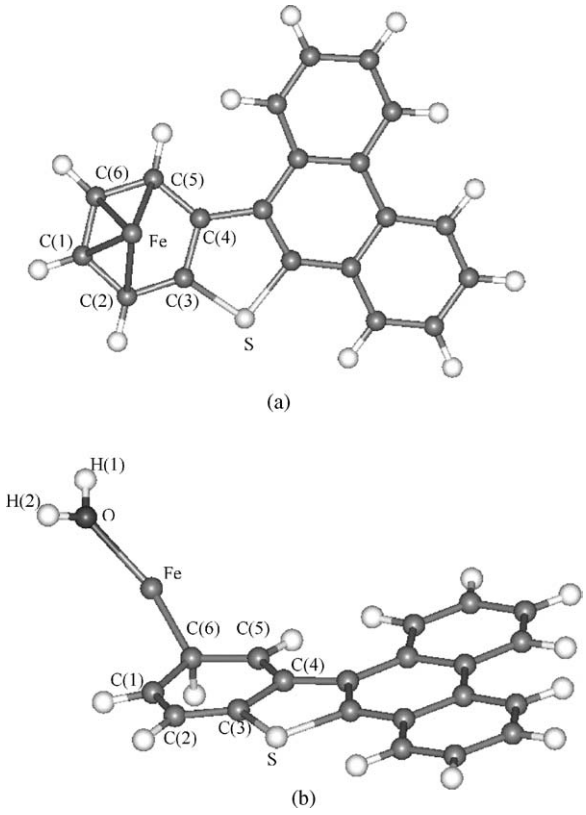

Fig. 5. (a) Adsorption mode of Fe on site A of fragment F2. (b) Final location of water molecule and Fe after interaction $H_2O–[F2–Fe]^0$. Note that Fe was initially on site A.

Table 4
DEs (a.u.), EBDs (Å), and DBE (kcal/mol) for interactions of Fe on site A of the F2 fragment with and without a water molecule (see Fig. 5)

Bonds	F2	$[F2–Fe]^0$	$[F2–Fe]^{-1}$	$[F2–FeH_2O]^0$	$[F2–FeH_2O]^{-1}$
Fe─C(1)	–	−0.102 (2.293) [−23.7]	−0.106 (2.264) –	−0.012 (2.807) [−2.7]	–
Fe─C(2)	–	−0.070 (2.414) [−16.6]	−0.079 (2.382) –	0.000 (4.020) [0.0]	–
Fe─C(5)	–	−0.100 (2.306) [−23.2]	−0.105 (2.279) –	0.002 (2.974) [0.4]	–
Fe─C(6)	–	−0.101 (2.259) [−23.8]	−0.115 (2.231) –	−0.438 (1.852) [−96.8]	–
C(3)─C(4)	−0.697 (1.439) [−115.0]	−0.662 (1.460) [−103.0]	−0.629 (1.475) –	−0.644 (1.461) [−110.7]	0.652 (1.462) –
C(5)─C(6)	−0.754 (1.396) [−130.5]	−0.699 (1.428) [−109.4]	−0.696 (1.430) –	−0.545 (1.517) [−94.1]	−0.741 (1.407) –
Fe─O	–	–	–	−0.328 (2.091) [−70.2]	−0.242 (2.177) –
O─H(1)	–	–	–	−0.487 (0.954) [−66.4]	−0.4891 (0.955) –
Iron charge		0.19	0.17	0.24	−0.22

Values of EBDs are in parentheses and DBE in brackets.

The interaction of Fe on site F leads, after geometrical optimization, to site E, shown in Fig. 6. This site presents very interesting features: strong interaction Fe–S (about −104 kcal/mol) and a sharp decrease of S–C(8) bond strength from about −101 to −27 kcal/mol (see Table 5). The EBD changes from 1.753 to 2.075 Å show an important enlargement of S–C(8) bond. These results strongly suggest that the S–C(8) bond may be broken during a thermal treatment and this may lead to a subsequent sulfur elimination in the presence of a hydrogen source (HDS). The S–C(3) bond is also activated (from −102 to −84 kcal/mol) but in less extent.

The effect of a negative charge on the F2–Fe system produces a weakening of interaction with the hydrocarbon, i.e., values of Fe–S interaction change from −0.493 a.u. in the neutral system to −0.306 a.u. in the charged one (see DE values in fist row of Table 5). In similar way, the EBD(Fe–S) is enlarged from 2.182 to 2.399 Å. A strengthening of the S–C(8) bond from −0.132 to −0.410 a.u. is also observed with its respective EBD shortage from about 2.075 to 1.795 Å.

For Fe in site E of fragment F2, the highest electronic charge transfer occurs from the Fe atom (0.74 a.u.) to the asphaltene fragment. A negative charge on the system decreases the Fe charge to 0.12 a.u. (see last row of Table 5). This transferred electronic charge is mainly located on the S atom.

3.3. Interaction asphaltene–Fe complexes (F1–Fe and F2–Fe) with water

The main goal of this work is to study the possibility of hydrogenation of unsaturated hydrocarbon species present in HO. In fact, a recent review shows that dispersed or immobilized transition metal nanoparticles have been used as catalyst for hydrogenation reactions of unsaturated hydrocarbonds [36]. In addition, aquathermolysis of organic compounds using superheated water can be used for transforming hydrocarbons [37]. Thus, water interaction on $[F1–Fe]^n$ and $[F2–Fe]^n$ complexes were evaluated considering neutral and negatively ($n = 0$ and −1) charged systems.

Values of DE and EBD for selected pairs of atoms in $[F1–FeH_2O]^0$ and $[F1–FeH_2O]^-$ systems with Fe on site A are also shown in Table 2. Results reveal that water interaction with Fe causes a displacement of the iron atom from A to E site (see Fig. 3). Table 2 indicates that H_2O interaction strongly increases Fe–N bond from about −35 to −110 kcal/mol (see values in brackets). The Fe–C(33) bond is maintained (−23 kcal/mol) and a new interaction Fe–C(28) of about −24 kcal/mol appears. On the other hand, N–C(33) is activated from about −113 in F1 to −71 in $[F1–FeH_2O]^0$, respectively. This is reflected in longer EBD(N–C(33)) (1.461 Å) in $[F1–FeH_2O]^0$ than those in F1 and $[F1–Fe]^0$ (1.305 and 1.400 Å, respectively) (see values in parentheses in row nine of Table 2).

The interaction of H_2O with Fe shows the formation of a Fe–O bond (DBE = −73 kcal/mol). An important activation of O–H bonds from a DBE of about −111 kcal/mol and EBD of 0.948 Å in the free H_2O molecule (see values in braces for O–H bonds in Table 2) to about −68 kcal/mol and 0.952 Å in $[F1–FeH_2O]^0$, respectively. These results suggest that there is the possibility to activate water O–H bonds by the interaction with Fe site adsorbed on heteroatoms of aromatic systems, such as asphaltenes.

Water adsorption on site A of the negative charged system reveals a notable decrease of Fe–N bond strength (see DE

Table 5
DEs (a.u.), EBDs (Å), and DBE (kcal/mol) for interactions of Fe on site E of the F2 fragment with and without water (see Fig. 6)

Bonds	F2	$[F2–Fe]^0$	$[F2–Fe]^{-1}$	$[F2–FeH_2O]^0$	$[F2–FeH_2O]^{-1}$
Fe─S	–	−0.493 (2.182) [−103.7]	−0.306 (2.399) –	−0.452 (2.216) [−80.7]	−0.498 (2.175) –
C(4)─C(3)	−0.697 (1.439) [−115.0]	−0.681 (1.446) [−115.3]	−0.651 (1.461) –	−0.679 (1.448) [−114.8]	−0.648 (1.464) –
S─C(3)	−0.462 (1.750) [−102.4]	−0.453 (1.757) [−83.9]	−0.426 (1.778) –	−0.465 (1.752) [−85.5]	−0.450 (1.758) –
S─C(8)	−0.458 (1.753) [−100.6]	−0.132 (2.075) [−26.7]	−0.410 (1.795) –	−0.149 (2.033) [−29.8]	−0.132 (2.072) –
Fe─O	–	–	–	−0.301 (2.119) [−62.1]	−0.275 (2.141) –
O─H(1)	–	–	–	−0.492 (0.953) [−70.5]	−0.497 (0.949) –
Iron charge	–	0.74	0.12	0.53	0.45

EBD and DBE values are in parentheses and brackets, respectively.

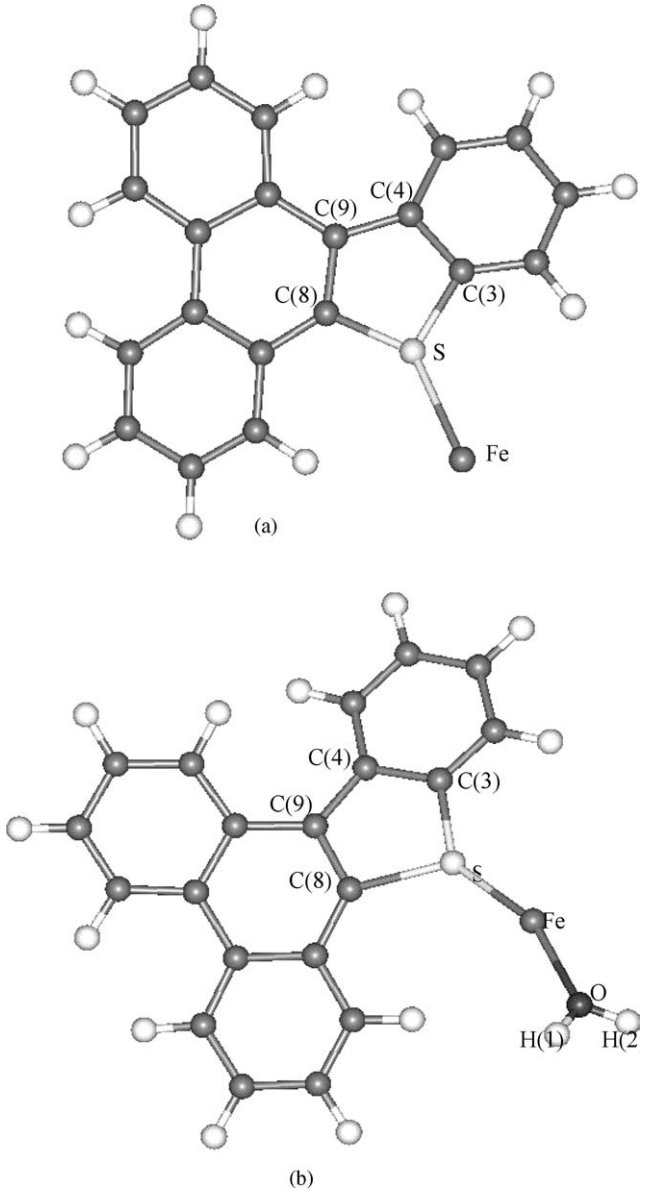

Fig. 6. (a) Adsorption mode of Fe on site E of fragment F2. (b) Final location of water molecule and Fe after interaction H_2O–$[F2–Fe]^0$.

changes from −0.506 to −0.341 a.u. in Table 2). A reinforcement of the Fe–C(34) bond from −0.001 to −0.305 a.u. with respect to that in $[F1–FeH_2O]^0$ complex also leads to a weakening of the C(34)–C(32) bond from −0.601 to −0.490 a.u., respectively. With respect to Fe–O, negative electronic charge leads to a small weakening of the Fe–O bond.

Results for interaction of H_2O with Fe adsorbed on site E of F1 are shown in Table 3. The neutral case is not discussed here, because, as mentioned above, adsorption on site A is transformed in an adsorption site similar to E. In the case of the negatively charged system, the Fe–N, Fe–C(28), and Fe–C(33) interactions decrease from −0.506, −0.103, and −0.113 a.u. in $[F1–FeH_2O]^0$ to −0.364, −0.048, and −0.065 a.u. in $[F1–FeH_2O]^-$, respectively. The iron atom becomes negatively charged (see last row of Table 3). So, the electronic charge donation does not favor the C–N and O–H activations due to a decrease of Fe–N and Fe–O bond strengths.

Interactions of water with Fe adsorbed on site A of F2 are presented in Table 4. Results of DBEs indicate that H_2O interaction on Fe breaks all Fe–C bonds, except the Fe–C(6) that goes from about −24 to −97 kcal/mol (see fifth row in Table 4 and Fig. 5b). This result correlates well with the EBD change of Fe–C(6) from 2.259 Å in $[F2–Fe]^0$ to 1.852 Å in $[F2–FeH_2O]^0$. The negative charge on the system ($[F2–FeH_2O]^{-1}$) produces a release of $FeOH_2$ from the asphaltene, as shown in the last column of Table 4.

Adsorption strengths of H_2O on $[F2–Fe]^0$ located on site E are displayed in Table 5. Water adsorption (see Fig. 6) weakens the Fe–S bond from about −104 to −81 kcal/mol. The Fe–O interaction (−62 kcal/mol) is smaller than in the rest of cases asphaltene–Fe–OH_2 interactions (−73 and −63 in sites A and E of F1 fragments, respectively, and −70 kcal/mol for site A of fragment F2; see Tables 2–4). Table 5 shows that the weakening of Fe–S bond is reflected in an enlargement of the EBD(Fe–S) from 2.182 to 2.216 Å. This, as expected, causes a decrease of the C–S activation.

The effect of negatively charged systems produces a strengthening of the Fe–S bond (from −0.452 to −0.498 a.u.), a smaller EBD(Fe–S) (from 2.216 to 2.175 Å), and a higher activation of S–C bonds (e.g., a decrease of DE(S–C(8) from −0.149 to −0.132 a.u. and an enlargement of this bond from 2.033 to 2.072 Å), than for the neutral system. The Fe–O bond, as in other cases, is weakened.

3.4. Comparison of asphaltene–Ni with asphaltene–Fe interactions

Differences and similarities between results of this work with those of previous investigations [6], using a model of Ni catalyst, are presented as follows:

1. The interaction of Ni and Fe with asphaltenic fragments F1 and F2 leads to relatively strong bonds that produce in both cases a weakening of C–N and C–S bonds of aromatic systems. It means that is feasible bond activations that facilitate HDN and HDS in presence of hydrogen.
2. The most important bonding interactions between Fe–asphaltene and Ni–asphaltene occur directly through heteroatoms (S and N atoms). However, in the case of Fe, formation of relevant Fe–C interactions takes place through carbon aromatic rings.
3. The interaction between water with negatively charged or neutral complexes $[F1–Ni]^0$ or $[F2–Ni]^0$ produces the water dissociation together with the hydrogen transference from the dissociated H_2O on Ni atom to the asphaltene [6]. In the case of water interaction on $[F1–Fe]^0$, $[F1–Fe]^{-1}$, $[F2–Fe]^0$, and $[F2–Fe]^{-1}$, O–H bond is activated but not broken.
4. The water interaction with the neutral and charged intermediates ($[F2–Ni]^0$ and $[F2–Ni]^{-1}$) produces the scission of one of the S–C bonds. The interaction with Fe leads only to a high S–C bond activation.

4. Comments and conclusions

In this work an upgrade of HO reaction is modeled by using a very simple model of Fe catalyst interacting with an asphaltene molecule model under the presence of water and electron-donor promoters (negative charged systems). The following qualitative conclusions were obtained from the analysis of metal–asphaltene bond interactions:

(a) Bonding interactions of Fe–asphaltene occur on aromatic rings or directly on the heteroatom, forming intermediate complexes. In the former case, multiple bonds with carbon atoms and heteroatoms are formed. There are several experimental and theoretical evidences that support these results. In general, Fe–X (X = N, S) bonds are stronger than Fe–C. These interactions, in most cases, cause a decrease of C–C, N–C, and S–C bond strengths (bond activations). This suggests possible cracking, HDS, and HDN processes due to asphaltene–metal bonding interactions.
(b) Electron transfer from the metal to the aromatic ring occurs after Fe–asphaltene interaction, except for adsorption on N atom.
(c) Water adsorption on the Fe–asphaltene complex metallic site leads to a weakening or activation of the O–H bonds. However, Fe is not able to split O–H bond as it occurs in the Ni metal.
(d) Reactivity of asphaltene with Fe as catalyst is smaller than that evaluated for Ni. Activation of water and C–X (X = N, S) bonds are lesser than in the case of Ni catalyst.
(e) Negatively charged systems ($[F1–Fe]^-$) and ($[F2–Fe]^-$) strengthen Fe–N and weaken Fe–S bonds, respectively, with respect to the neutral ones. On the other hand, $[F1–FeOH_2]^-$ and $[F2–FeOH_2]^-$ weaken Fe–N and strengthen Fe–S bonds, respectively, with respect to the neutral ones. In the case of Fe adsorption on six-carbon ring with H_2O, the negative charge leads to the formation of a $FeOH_2$ complex out of the asphaltene surface.
(f) It is important to note that a more realistic model of the catalyst must be considered. Thus, the evaluation of different cluster sizes for Fe and Ni is in progress in order to obtain correlation with actual experimental catalysts. It is also important to consider the formation of M_n–O_m clusters (M = Ni, Fe).

Acknowledgments

This research has been partially sponsored by FONACIT, Venezuela, under contract G-9700667. We also thank Professor Claudio Mendoza for revising our manuscript.

References

[1] P. Pereira, I. Machín, G. Salerno, E. Cotte, I. Higuerey, A. Andriollo, J. Córdoba, l. Zacarías, R. Marzín, G. Rivas, Acta Cient. Venez. 50 (1999) 48.
[2] P. Pereira, R. Marzín, L. Zacarías, I.L. Trosell, F. Hernández, J. Córdova, J. Szeoke, C. Flores, J. Duque, R.B. Solari, Visión Tecnológica 6 (5) (1998).
[3] D.C. Grenouble, J. Catal. 75 (1982) 51.
[4] D. Duprez, J. Catal. 90 (1984) 292.
[5] G. Gambús, P. Patiño, J. Navea, Energy Fuels 16 (2002) 172.
[6] I. Machín, F. Ruette, A. Sierraalta, J.C. de Jesús, G. Rivas, I. Higuerey, J. Córdova, P. Pereira, J. Mol. Catal. A 227 (2005) 223.
[7] F. Ruette, M. Sanchez, G. Martorell, C. Gonzalez, R. Añez, A. Sierraalta, L. Rincón, C. Mendoza, Int. J. Quantum Chem. 96 (2004) 321.
[8] F. Ruette, M. Sánchez, C. Mendoza, A. Sierraalta, G. Martorell, C. González, Int. J. Quantum Chem. 96 (2004) 303.
[9] F. Ruette, C. González, Chem. Phys. Lett. 359 (2002) 428.
[10] R. Martínez, F. Brito, M.L. Araujo, F. Ruette, A. Sierraalta, Int. J. Quantum Chem. 97 (2004) 854.
[11] C. Mendoza, F. Ruette, G. Martorell, L.S. Rodrígues, Astron. Astrophys. 601 (2004) L59.
[12] M. Romero, M. Sánchez, A. Sierraalta, L. Rincón, F. Ruette, J. Chem. Inf. Comput. Sci. 39 (1999) 543.
[13] F. Ruette, C. González, A. Octavio, J. Mol. Struct. (Theochem) 537 (2001) 17.
[14] F. Ruette, S.A.M. Marcantognini, V.V. Karasiev, J. Mol. Struct. (Theochem) 636 (2003) 15.
[15] G. Blyholder, J. Head, F. Ruette, Theor. Chim. Acta 60 (1982) 429.
[16] L.J. Rodríguez, F. Ruette, M. Rosa-Brussin, J. Mol. Catal. 62 (1990) 199.
[17] M. Sánchez, F. Ruette, A.J. Hernández, J. Phys. Chem. 96 (1992) 823.
[18] O. Hübner, V. Termath, A. Berning, J. Sauer, Chem. Phys. Lett. 294 (1998) 37.
[19] D. Linde, CRC Handbook of Chemistry and Physics, 72nd ed., Boca Raton, FL, 1998, pp. 9–54.
[20] D.J. Brugh, M.D. Morse, J. Chem. Phys. 107 (1997) 9772.
[21] D. Schröder, I. Kretzschmar, H. Schwarz, C. Rue, P.B. Armentrout, Inorg. Chem. 38 (1999) 3474.
[22] A. Fiedler, S. Iwata, J. Phys. Chem. A 102 (1998) 3618.
[23] X. Xu, X. Lü, N. Wang, Q. Zhang, M. Ehara, H. Nakatsuji, Int. J. Quantum Chem. 72 (1999) 221.
[24] D. Linde, CRC Handbook of Chemistry and Physics, 72nd ed., Boca Raton, FL, 1998, pp. 9–18.
[25] J.R. Primera, M. Romero, M. Sánchez, A. Sierralta, F. Ruette, J. Mol. Struct. (Theochem) 469 (1999) 177.
[26] M. Sanchez, F. Ruette, J. Mol. Struct. (Theochem) 254 (1992) 335.
[27] F. Ruette, F.M. Poveda, A. Sierraalta, J. Rivero, Surf. Sci. 349 (1996) 241.
[28] I. Higuerey, Comparative study of product distribution of thermal cracking reactions and steam cracking of Tia Juana heavy oil residuals, Ph.D. Thesis, Universidad Central de Venezuela, 2001.
[29] D. Caraiman, D.K. Bohme, J. Phys. Chem. A 106 (2002) 9705.
[30] E. Hegenberger, N.L. Wu, J. Phillips, J. Phys. Chem. 91 (1987) 5067.
[31] F. Meyer, F.A. Khan, P.B. Armentrout, J. Am. Chem. Soc. 117 (1995) 9740.
[32] R. Pandey, B.K. Rao, P. Jena, M. Alvarez-Blanco, J. Am. Chem. Soc. 123 (2001) 3799.
[33] J. Molina-Molina, J.A. Dobado, S. Melchor, J. Mol. Struct. (Theochem) 589–590 (2002) 337.
[34] C.W. Bauschlicher, H. Partridge, S.R. Langhoff, J. Phys. Chem. 96 (1992) 3273.
[35] K. Schroeter, R. Wesendrup, H. Schwarz, Eur. J. Org. Chem. (1998) 565.
[36] A. Roucoux, J. Schulz, H. Patin, Chem. Rev. 102 (2002) 3757.
[37] A.R. Katritzky, S.M. Allin, M. Siskin, Acc. Chem. Res. 29 (1996) 399.